http://dx.doi.org/10.5012/bkcs.2012.33.1.65

Electrochemical Properties of $Li_{1.1}V_{0.75}W_{0.075}Mo_{0.075}O_2$/Graphite Composite Anodes for Lithium-ion Batteries

Hyung Sun Kim,* Sang-Ok Kim, Yong-Tae Kim,† Ji Kwon Jung,‡ Byung Ki Na,‡ and Joong Kee Lee

Energy Storage Research Center, Korea Institute of Science and Technology (KIST), Seoul 130-650, Korea
**E-mail: kimhs@kist.re.kr*
†School of Mechanical Engineering, Pusan National University, Busan 609-735, Korea
‡Department of Chemical Engineering, Chungbook National University, Cheongju 361-763, Korea
Received August 26, 2011, Accepted October 31, 2011

Novel type $Li_{1.1}V_{0.9-2x}W_xMo_xO_2$ powders were prepared by a solid-state reaction of Li_2CO_3, V_2O_3, WO_2 and MoO_2 precursors in a nitrogen atmosphere containing 10 mol % hydrogen gas, and assessed as anode materials in lithium-ion batteries. The specific charge and discharge capacities of the $Li_{1.1}V_{0.9-2x}W_xMo_xO_2$ anodes were higher than those of the bare $Li_{1.1}V_{0.9}O_2$ anode. The cyclic efficiency of these anodes was approximately 73.3% at the first cycle, regardless of the presence of W and Mo doping. The composite anode, which was composed of $Li_{1.1}V_{0.75}W_{0.075}Mo_{0.075}O_2$ (20 wt %) and natural graphite (80 wt %), demonstrated reasonable specific capacity, high cyclic efficiency, and good cycling performance, even at high rates without capacity fading.

Key Words : $Li_{1.1}V_{0.9-2x}W_xMo_xO_2$, Composite anode, Lithium-ion batteries

Introduction

Vanadium-based oxides are considered promising anode materials for lithium-ion batteries.[1-3] Among these materials, $Li_{1.1}V_{0.9}O_2$ was recognized as a potential alternative anode to graphite.[4-7] $Li_{1.1}V_{0.9}O_2$ has double the volumetric capacity than commercial graphite under charging conditions of 0.01V *vs.* Li/Li^+. In addition, the energy density of the cell based on this material could be enhanced significantly because of its low working potential of < 0.3 V *vs.* Li/Li^+ during the charge and discharge reactions. The potential of this material as a high-density anode electrode has prompted intensive research on its structure and valence state. $Li_{1.1}V_{0.9}O_2$ has an ordered layered crystalline structure with Li^+ and V^{+3} ions occupying alternate (111) planes, and exhibits a hexagonal structure.[8,9] After lithium intercalation, $Li_{1.1}V_{0.9}O_2$ is converted to $Li_{2.1}V_{0.9}O_2$, corresponding to the *P*-3m1 space group, and the oxidation state of vanadium ions is reduced from V(III) to V(II). The layered structure of $Li_{1.1}V_{0.9}O_2$, gives it a relatively low volume change of 25% during the cycling process compared to that of highly capacitive silicon or tin-based anode materials. On the other hand, the electrochemical properties of $Li_{1.1}V_{0.9}O_2$ might be insufficient for high-current applications owing to its low conductivity. Therefore, surface modification or other treatment methods should be applied to enhance the rate capability. Metal doping is one of the most effective methods for improving the electrochemical properties of $Li_{1.1}V_{0.9}O_2$. W and Mo-based oxide materials are used as dopants for $Li_{1.1}V_{0.9}O_2$, which is used as an anode material in lithium-ion batteries.[10,11] These metals are suitable for the preparation of high-density anodes because of their high intrinsic density, low cost and non-toxic environment.

In this study, a simple solid-state reaction was used to prepare a conducting $Li_{1.1}V_{0.9-2x}W_xMo_xO_2$ anode material using a metal doping process. The electrochemical properties of the anodes of these lithium-ion batteries were examined using a range of analytical techniques.

Experimental

The $Li_{1.1}V_{0.9-2x}W_xMo_xO_2$ (x = 0, 0.025, 0.05, 0.075, 0.1) samples were prepared by sintering an intimate mixture of the required quantities of Li_2CO_3 (Aldrich, 98%), V_2O_3 (Alfa Aesar, 99.7%), WO_2 (Aldrich, 99.8%), and MoO_2 (Aldrich, 99.8%) precursors under flowing N_2 gas containing 10 mol % H_2 at 500 °C for 6 h and then at 1100 °C for 10h at a heating rate of 5 °C/min in the same atmosphere. The active materials were then allowed to cool naturally to room temperature. The electrodes were prepared by mixing the active materials (80 wt %), conducting materials (Denka Black, 10 wt %), a mixture of styrene butadiene rubber (40 wt % in water, Sigma) and sodium carboxymethyl cellulose (1 wt % in water, Zeon) binder (10 wt %). The slurry was cast on copper foil, dried at 80 °C in a vacuum oven for 24 h to remove the residual solvent, and pressed using a rolling machine. The composite anodes were prepared by planetary ball-milling $Li_{1.1}V_{0.75}W_{0.075}Mo_{0.075}O_2$ and natural graphite at different weight ratios under the above conditions. These composite anodes were assembled with a lithium foil electrode using CR2032 coin cells in a dry room (dew point: −60 °C). The electrolyte was 1 M $LiPF_6$ in a solvent mixture containing ethylene carbonate and dimethyl carbonate (3:7 by volume ratio). A microporous polypropylene separator (Celgard 2400) was used. The crystal structure of $Li_{1.1}V_{0.9-2x}W_xMo_xO_2$ powders was analyzed by X-ray diffraction (XRD, Rigaku D/MAX-2500V). The morphology of the graphite and composite powders was examined by

scanning electron microscopy (SEM, Hitachi 4300). The ac impedance measurements were performed over the frequency range, 1 MHz to 0.1 Hz using a Solartron 1260 frequency response analyzer coupled with a 1286 electrochemical interface. The cyclic properties of the cells were examined by galvanostatic modes at voltages ranging from 0.005 to 2.0V *vs*. Li/Li$^+$ using a Maccor cycle system (S 4000 series).

Results and Discussion

Figure 1 shows the initial charge and discharge voltage curves of the $Li_{1.1}V_{0.9-2x}W_xMo_xO_2$ (x = 0, 0.025, 0.05, 0.075, 0.1) anodes at a 0.1C rate (3 mA current). During the initial lithium intercalation, the two plateau potentials at 0.58 V and 0.1 V *vs*. Li/Li$^+$ were observed in the bare $Li_{1.1}V_{0.9}O_2$ anode as well as the W and Mo-doped $Li_{1.1}V_{0.9}O_2$ anodes. However, the voltage curve shape of $Li_{1.1}V_{0.7}W_{0.1}Mo_{0.1}O_2$ anode is different from that of other metal-doped $Li_{1.1}V_{0.9}O_2$ anodes. This effect could be attributed to the structural change of original $Li_{1.1}V_{0.9}O_2$ anode material by excess metal doping. The specific charge and discharge capacities of the W and Mo-doped $Li_{1.1}V_{0.9}O_2$ anodes were higher than those of the bare $Li_{1.1}V_{0.9}O_2$ anode except $Li_{1.1}V_{0.7}W_{0.1}Mo_{0.1}O_2$ anode. The cyclic efficiency of these anodes was approximately 73.3% in the first cycle, irrespective of metal doping. The rate capability of the $Li_{1.1}V_{0.9-2x}W_xMo_xO_2$ (x = 0, 0.025, 0.05, 0.075) anodes based on the specific charge capacity was also summarized in Table 1. Among these anodes, $Li_{1.1}V_{0.75}W_{0.075}Mo_{0.075}O_2$ anode showed the best rate capability even at high rates.

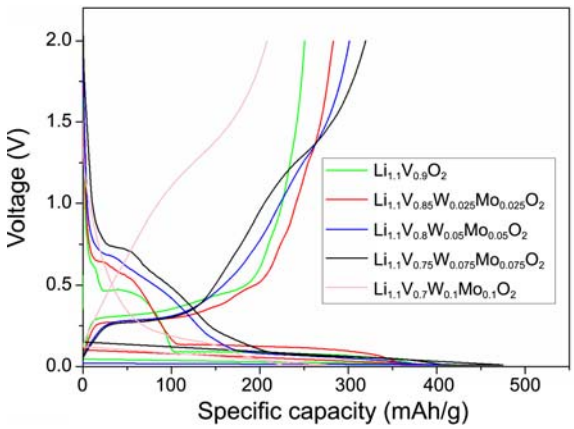

Figure 1. Initial charge and discharges voltage curves of the bare $Li_{1.1}V_{0.9}O_2$ and $Li_{1.1}V_{0.9-2x}W_xMo_xO_2$ anodes at a 0.1C rate.

Table 1. The rate capability of the $Li_{1.1}V_{0.9-2x}W_xMo_xO_2$ (x = 0, 0.025, 0.05, 0.075) anodes

Sample	0.1C rate	1C rate	5C rate
$Li_{1.1}V_{0.9}O_2$	252 mAh/g	191 mAh/g	82 mAh/g
$Li_{1.1}V_{0.85}W_{0.025}Mo_{0.025}O_2$	270 mAh/g	208 mAh/g	122 mAh/g
$Li_{1.1}V_{0.8}W_{0.05}Mo_{0.05}O_2$	300 mAh/g	227 mAh/g	136 mAh/g
$Li_{1.1}V_{0.75}W_{0.075}Mo_{0.075}O_2$	325 mAh/g	249 mAh/g	152 mAh/g

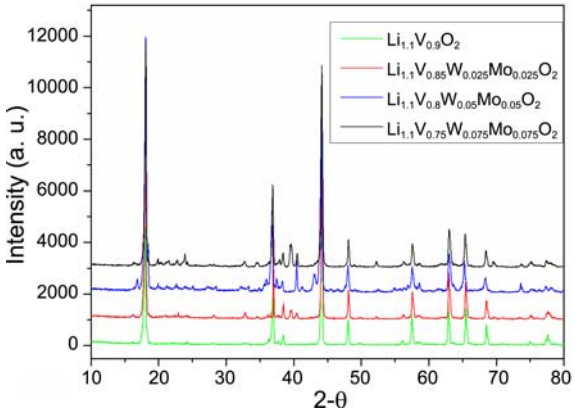

Figure 2. XRD patterns of the synthesized $Li_{1.1}V_{0.9-2x}W_xMo_xO_2$ powders.

Table 2. Lattice parameters of $Li_{1.1}V_{0.9-2x}Mo_xW_xO_2$ powders (x = 0, 0.025, 0.05, 0.075)

Sample	a (Å)	c (Å)	c/a
$Li_{1.1}V_{0.9}O_2$	2.8492	14.6967	5.1582
$Li_{1.1}V_{0.85}W_{0.025}Mo_{0.025}O_2$	2.8494	14.6682	5.1478
$Li_{1.1}V_{0.8}W_{0.05}Mo_{0.05}O_2$	2.8526	14.6675	5.1418
$Li_{1.1}V_{0.75}W_{0.075}Mo_{0.075}O_2$	2.8528	14.6666	5.1411

As shown in Figure 2, the XRD patterns on the bare $Li_{1.1}V_{0.9}O_2$ powder and $Li_{1.1}V_{0.9-2x}Mo_xW_xO_2$ powders demonstrated that they have a layered structure (space group R-3m), irrespective of the presence of metal doping. Table 2 lists the lattice parameters of the synthesized $Li_{1.1}V_{0.9-2x}Mo_xW_xO_2$ powders. The cell parameters of a and c were changed slightly by W and Mo doping. The lattice parameter of the a-axis increased with increasing W and Mo concentration, whereas that of the c-axis decreased. That is, the atomic bond length between the atoms in the same layer increased, whereas the interaction between each layer became stronger.

The impedance properties of these anodes were investigated to gain a better understanding of the doping effect of $Li_{1.1}V_{0.9}O_2$ anodes on the electrochemical performance. The ac voltage used during the measurements was 10 mV. The impedance spectra of the bare $Li_{1.1}V_{0.9}O_2$ and metal-doped $Li_{1.1}V_{0.9}O_2$ anodes in Figure 3 show the lines intercepting the real part at high frequency, corresponding to the electrolyte resistance. The first semicircle at high frequency represents the resistance of the solid state interface layer formed on the electrode surface. The second semicircle at the middle frequency corresponds to faradic charge transfer resistance. Therefore, the decrease in the diameter of the second semicircle can be attributed to the decreased charge transfer resistance of the lithium intercalation reaction by metal doping. Among these anodes, the $Li_{1.1}V_{0.75}W_{0.075}Mo_{0.075}O_2$ anode showed the lowest interfacial resistance and highest specific capacity during cycling. Therefore, $Li_{1.1}V_{0.75}W_{0.075}Mo_{0.075}O_2$ powder is a suitable anode material for lithium-ion batteries, and can be used as a composite anode with natural

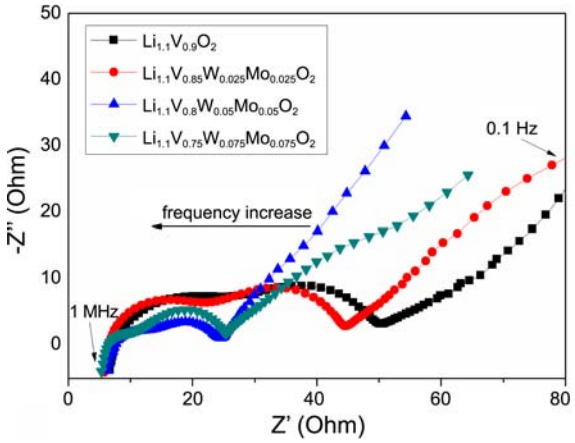

Figure 3. Electrochemical impedance spectrum of the bare $Li_{1.1}V_{0.9}O_2$ and $Li_{1.1}V_{0.9-2x}W_xMo_xO_2$ anodes after the 1st cycle.

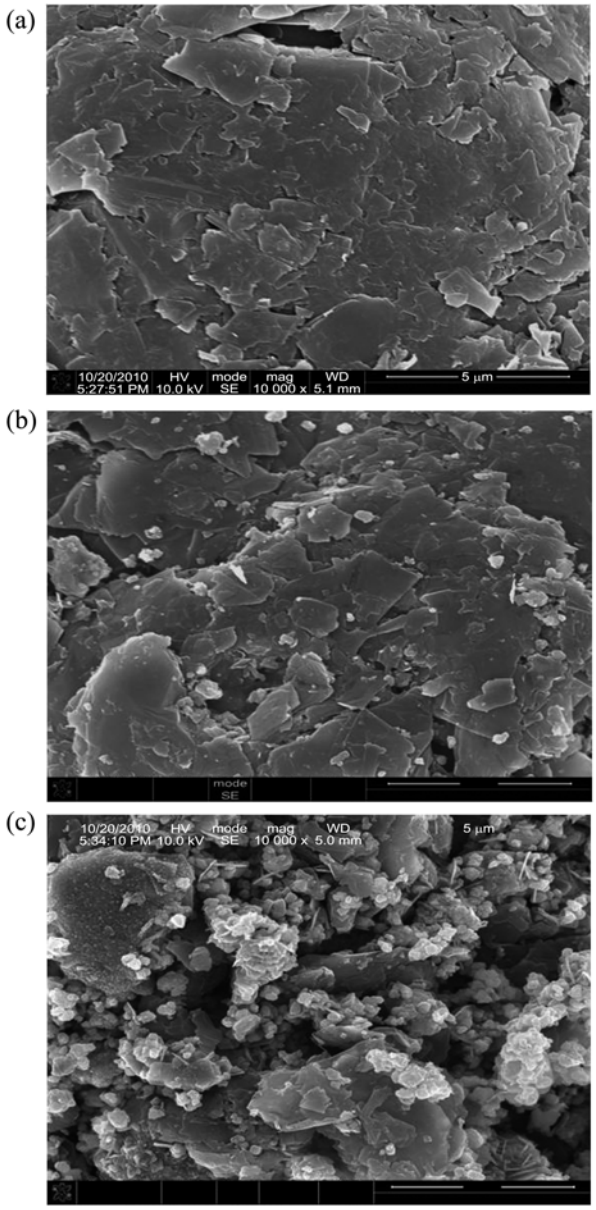

Figure 4. SEM images of the graphite and composite anode materials (A: graphite, B: S1, C: S2).

graphite powder to achieve a good cycling stability. Figure 4 shows SEM images of the $Li_{1.1}V_{0.75}W_{0.075}Mo_{0.075}O_2$ and graphite composite powders with different weight ratios. The sample names are as follows:

S1 ($Li_{1.1}V_{0.75}W_{0.075}Mo_{0.075}O_2$: natural graphite = 20:80 wt %) and S2 ($Li_{1.1}V_{0.75}W_{0.075}Mo_{0.075}O_2$: natural graphite = 50:50 wt %). The obtained $Li_{1.1}V_{0.75}W_{0.075}Mo_{0.075}O_2$ powder has a mean size of approximately 2-3 μm with spherical features. They could be dispersed well and embedded within the graphite matrix, as shown in S1 and S2. Figure 5 shows the charge and discharge voltage curves of the graphite anode and other composite anodes at a 0.1C current rate in the first cycle. The specific charge and discharge capacities of the graphite anode were 350 mAh/g and 360 mAh/g, respectively, and the cyclic efficiency was approximately 97.2%. During the first lithium intercalation, the plateau potential at 0.58V *vs*. Li/Li^+ observed in the pure $Li_{1.1}V_{0.9}O_2$ anode was not observed clearly in the S1 and S2 composite anodes. This plateau potential can be related to the irreversible capacity to form a solid electrolyte interphase on the anode surface.[5] Therefore, the cyclic efficiency of this composite anode was similar to that of the graphite anode due to the disappearance of a side reaction in the first cycle. The specific charge and discharge capacities of the S1 and S2 composite anodes were slightly higher than those of the graphite anode at the same rate. On the other hand, the curve pattern of the charge potential of these composite anodes showed a slope line in the voltage range of 0.25 V and 2 V *vs*. Li/Li^+ due to the presence of a $Li_{1.1}V_{0.75}W_{0.075}Mo_{0.075}O_2$ anode material in the composite anode. Consequently, these results imply that $Li_{1.1}V_{0.9}O_2$ anode with an ordered layered structure could be slightly changed by the addition of W and Mo. In contrast, the curve pattern of the charge potential of the graphite electrode showed a straight line in the same voltage range. When compared with $Li_{1.1}V_{0.75}W_{0.075}Mo_{0.075}O_2$ anode, the increased specific capacity of S1 and S2 composite anodes could not be explained clearly. Probably, this effect may be attributed to the change into $Li_{2.1+y}V_{0.75}W_{0.075}Mo_{0.075}O_2$ during the cycling by the addition of graphite. Figure 6 shows the charge and discharge voltage curves of

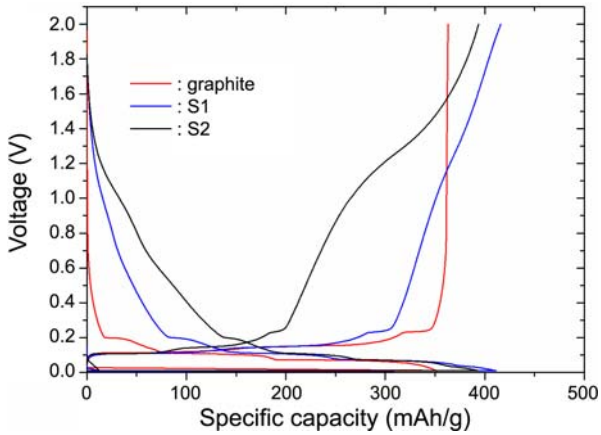

Figure 5. Charge and discharge voltage curves of graphite and composite anodes at a 0.1C rate.

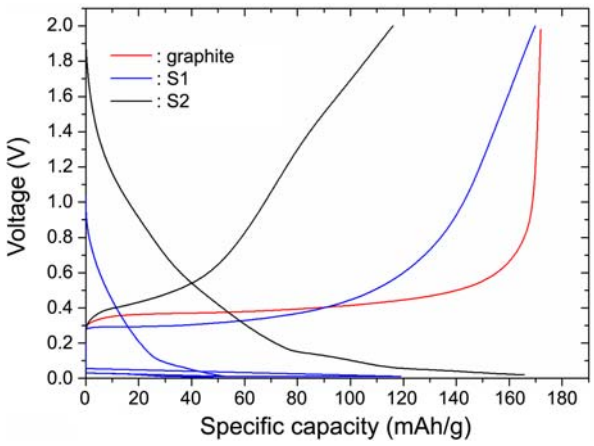

Figure 6. Charge and discharge voltage curves of the graphite and composite anodes at a 2C rate.

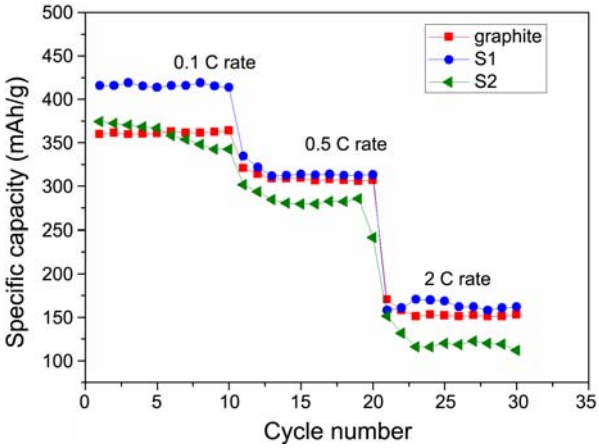

Figure 7. Cycling performance of the graphite and various composite anodes at different rates.

the graphite anode and other composite anodes at a high current rate (2C rate). The specific capacities of the graphite anode and S1 composite anode were 170 mAh/g and the cyclic efficiency was approximately 97.2%. This suggests that the $Li_{1.1}V_{0.75}W_{0.075}Mo_{0.075}O_2$ anode material acts satisfactory as an active matrix for the charge and discharge reaction without capacity loss, even at a high rate. On the other hand, the charge plateau potential of the S2 composite anode disappeared in the entire voltage range and the specific charge capacity decreased to 100 mAh/g. This might be due to the lower rate capability of the $Li_{1.1}V_{0.75}W_{0.075}Mo_{0.075}O_2$ anode compared to the graphite anode. Figure 7 shows the cycling performance of the composite anodes and graphite anode at different current rates. The specific capacities of the S1 composite anode were 420 mAh/g and 320 mAh/g at a 0.1C and 0.5C rate, respectively. This composite anode showed higher capacity than the graphite anode, even at a 2C rate. On the other hand, the specific capacity and cycling stability of the S2 composite anode were lower than those of the S1 composite anodes and graphite anode at all current rates. This might be due to the lower cycling stability of the $Li_{1.1}V_{0.9}O_2$ anode material compared to graphite.

Conclusion

$Li_{1.1}V_{0.9-2x}W_xMo_xO_2$ (x = 0, 0.025, 0.05, 0.075) anode materials were synthesized by a solid-state reaction. The W and Mo-doped $Li_{1.1}V_{0.9}O_2$ anodes showed higher specific capacities and lower polarization than the bare $Li_{1.1}V_{0.9}O_2$ anode during cycling. Among these anodes, the $Li_{1.1}V_{0.75}W_{0.075}Mo_{0.075}O_2$ anode showed the highest specific capacity and lowest interfacial resistance compared to the other $Li_{1.1}V_{0.9-2x}W_xMo_xO_2$ anodes. Composite anodes were prepared by ball-milling $Li_{1.1}V_{0.75}W_{0.075}Mo_{0.075}O_2$ and graphite powders at different weight ratios. The composite anode (S1) exhibited higher specific capacity than the graphite anode at a 0.1C rate and good cycling performance without capacity fading even at a 2C rate, making them a suitable alternative anode in lithium-ion batteries.

Acknowledgments. This study was funded by "The Middle and Long-term Technology Development Project" of the Ministry of Knowledge Economy of Korea.

References

1. Huang, W.; Gao, S.; Ding, X.; Jiang, L.; Wei, M. *J. Alloys and Compounds* **2010**, *495*, 185.
2. Reddy, M.; Pecquenard, B.; Vinatier, P.; Levasseur, A. *J. Power Sources* **2007**, *163*, 1040.
3. Morishita, T.; Nomura, K.; Inamasu, T.; Inagaki, M. *Solid State Ionics* **2005**, *176*, 2235.
4. Choi, N.; Kim, J.; Yin, R.; Kim, S. *Materials Chemistry and Physics* **2009**, *116*, 603.
5. Kim, H.; Cho, B. *Bulletin of the Korean Chemical Society* **2010**, *31*, 1267.
6. Lee, S.; Kim, H.; Seong, T. *J. Alloys and Compounds* **2011**, *509*, 3136.
7. Song, J.; Park, H.; Kim, K.; Jo, Y.; Kim, J.; Jeong, Y.; Kim, Y. *J. Power Sources* **2010**, *195*, 6157.
8. Goodenough, J.; Dutta, G.; Manthiram, A. *Physical. Review B* **1991**, *43*, 10170.
9. Yin, R.; Kim, Y.; Choi, W.; Kim, S.; Kim, H. *Advances in Quantum Chemistry* **2008**, *54*, 23.
10. Scrosati, B. *Electrochimica Acta* **1981**, *26*, 1559.
11. Schalkwijk, W.; Scrosati, B., *Advances in Lithium-Ion Batteries*; Kluwer Academic/Plenum Publishers: New York, 2002; Ch. 3.